We are IntechOpen, the world's leading publisher of Open Access books Built by scientists, for scientists

4,800
Open access books available

122,000
International authors and editors

135M
Downloads

Our authors are among the

154
Countries delivered to

TOP 1%
most cited scientists

12.2%
Contributors from top 500 universities

CLARIVATE ANALYTICS BOOK CITATION INDEX INDEXED

WEB OF SCIENCE™

Selection of our books indexed in the Book Citation Index in Web of Science™ Core Collection (BKCI)

Interested in publishing with us?
Contact book.department@intechopen.com

Numbers displayed above are based on latest data collected.
For more information visit www.intechopen.com

Chapter 4

Enhanced Transmission of Acoustic Waves Through Subwavelength Holes in Hard Plates

Bo Hou and Weijia Wen

Additional information is available at the end of the chapter

http://dx.doi.org/10.5772/54196

1. Introduction

In 1944, Bethe found the transmittance of electromagnetic (EM) waves through a tiny hole in a perfectly conducting screen varies as being proportional to $(kr)^4$, where $k=2\pi/\lambda$, λ is the wavelength and r is the hole radius [1]. This result shows that a small hole has extremely low transmission or negligible cross section for EM waves of very long wavelength. For a hole of finite thickness, the transmittance is found to be reduced further, because no propagating mode exists inside the hole [2].

However, in 1998, Ebbesen *et al.* has observed enhanced transmission of light through either a lattice of subwavelength holes or a single hole surrounded by surface periodical patterns on thin metallic films, where the optical transmission can be much larger than the area fraction of the holes at specific frequencies [3-13]. The holes, once organized or decorated, have the transmission cross section larger than themselves' area, which is different radically from the theory by Bethe. Since then, the remarkable phenomenon has inspired a tremendous amount of attention and works on resonant transmissions of EM waves through various apertures on either metallic or dielectric structure [14-25]. Phenomenologically, various observed transmission resonances are associated with two geometrical factors: structural factor (SF) emerging globally from the lattice periodicity and aperture factor owned locally by the individual unit [26-29]. Structural-factor-related resonances typically have the transmission wavelength comparable to the lattice constant and are dependent strongly on the incidence angle. In sharp contrast, aperture-factor-related resonances have the wavelength determined mainly by the transversal/longitudinal dimensions of the aperture and are not sensitive to the incidence angle.

It is well known that acoustic and EM waves share a lot of wave phenomena, but they have something in difference. In nature, acoustic wave is a scalar longitudinal wave in inviscid fluids, while EM wave is a vector transverse wave. Consequently, a subwavelength hole has no cutoff for acoustic wave, but does for EM wave, which underlies the distinct

transmissions of acoustic/EM waves through a hole in an ideally rigid/conducting screen. The acoustic transmission of a single hole approaches a constant, $8/\pi^2$, dislike the EM case, with decreasing the ratio r/λ [30].

Transmission/diffraction by an acoustical grating is an old problem, and the previous investigations addressed some cases: one-dimensional (1D) periodic slits in a rigid screen [31,32], a single hole in a thick wall [33,34], and a 1D grating composed of parallel steel rods with finite grating thickness [35,36]. Here we studied the acoustic transmissions through two structures: (1) a two-dimensional array (square lattice) of subwavelength hole and (2) a single hole surrounded by the surface periodic grooves. It is found that the acoustic transmission phenomenon for the structured thin plates is analogous completely to the case of EM wave, except for the transmission phase. For the hole array in thick plates, the transmission peaks are related to the Fabry-Perot-like (FP-like) resonances inside the holes and can occur to the frequencies well below Wood's anomalies.

2. Ultrasonic measurements

In our experiments, the measurements of far field transmissions of acoustic waves in the ultrasonic frequency regime (0.2–2.0 MHz) were performed in a large water tank. Two immersion transducers were employed as ultrasonic generator and receiver, and the sample was placed at a rotation stage located between the two transducers at an appropriate distance. The sample could be rotated, so that the oblique incidences were measured. The ultrasonic pulse was incident upon the sample and the transmitted signal was collected by the receiver, collinear with the incident wave. Transmission magnitude, T, and transmission phase, ϕ, of the sample were obtained by normalizing the Fourier transformed spectra of the signal through the sample, $\left|A_s(f)\right|\exp\left[j\phi_s(f)\right]$, with respect to the signal through the water background (without the sample in place), $\left|A_b(f)\right|\exp\left[j\phi_b(f)\right]$, where f is the frequency and $j^2=-1$. Consequently, $T=\left|A_s(f)/A_b(f)\right|$, and $\phi=\phi_s(f)-\phi_b(f)-2\pi f t/c$ (c =1490 m/s being the speed of acoustic wave in water, t being the sample thickness).

In the context, the term "transmission" when referring to the spectrum means the amplitude ratio, T, of the transmitted and the incident waves. To figure out whether the transmission is enhanced, we need calculate the ratio of transmitted energy flow to the energy flow incident on all holes. Within a unit cell of the hole array, the ratio can be expressed by:

$$\frac{I_t\cdot a^2}{I_i\cdot \pi d^2/4}=\frac{\left|A_t/A_i\right|}{\pi d^2/\left(4a^2\right)}=\frac{T^2}{\xi}=\frac{\mathcal{T}}{\xi} \tag{1}$$

where I_t (A_t) and I_i (A_i) denote the intensities (amplitudes) of transmitted and incident acoustic waves, respectively, a is the lattice constant, d is the hole diameter, and $\xi=\pi d^2/\left(4a^2\right)$ is the area fraction of the holes. We call the squared transmission magnitude T^2 as transmittance $\mathcal{T}$ representing the acoustic intensity transmission. If $\mathcal{T}/\xi>1$, then the enhanced transmission is obtained.

Apart from measuring the transmission spectrum, we also implemented point-by-point scanning to detect the pressure field distribution in the transmission process. A pinducer (1.5 mm in diameter) replaced the receiving transducer and was located at a distance, z, from the rear surface of the sample to detect the pressure field distribution there. The pinducer was mounted on a two-dimensional translation stage. The scanning was done along the x-y plane parallel to the sample surface, with a spatial step of 0.1mm×0.1mm.

3. Experimental results

3.1. Enhanced transmission of acoustic waves through hole array structure

First we measured the acoustic transmission of a hole array with the hole diameter d = 0.5 mm, the lattice constant a = 1.5 mm, and the plate thickness t = 0.5 mm. Figure 1 shows the transmittance of the hole array at normal incidence, compared to the transmittance of a smooth brass plate with identical thickness. For the smooth brass plate, very low transmittance is seen because of the acoustic impedance mismatch (η_{brass} / η_{water} ≈ 25). It is noticed that the transmittance rises at lower frequencies, which indicates a thin brass plate can not block acoustic waves of very long wavelength or very low frequency. This fact is different from the EM case where a sheet of metal as thin as skin depth works well. For the hole array, a pronounced peak is seen at 0.85 MHz and followed by a transmittance zero close to 1.0 MHz which is just Wood's anomaly λ=a. The peak has the transmittance (68%), much lager than the area fraction (8.7%) of holes occupation in the array structure, and shows an acoustic transmission enhancement through the hole array, similar to the EM case.

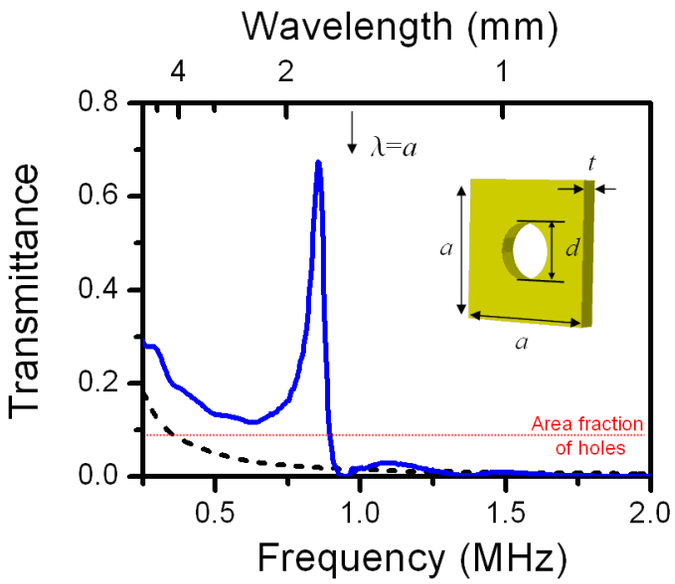

Figure 1. Transmittance of the acoustic waves at normal incidence through a hole array (solid line) and a smooth brass plate (dashed line) with the same thickness. The hole array has the parameters: the hole diameter d = 0.5 mm, the lattice constant a = 1.5 mm, and the plate thickness t = 0.5 mm. A schematic picture of the unit cell is illustrated as the inset. The level dot line represents the area fraction of holes in the array. Reprinted with permission from J. Appl. Phys. 104, 014909 (2008). Copyright 2008 American Institute of Physics.

We also investigated the dependence of the transmission peak on the lattice constant. Figure 2 shows the normal transmissions of the hole arrays with identical lattice constant a = 2.0 mm and different hole diameters. The transmission peak and two Wood's anomalies (pointed by arrows) are identified at ~0.75 MHz and ~1.1MHz. With the larger diameter holes (d = 1.2 mm), the peak becomes more pronounced. Comparing with the array of a = 1.5 mm in Figure 1, it is clear to show that the peaks and Wood's anomalies downshift to lower frequencies as the lattice constant increases. In Figure 2, we also plotted the measured transmission phase ϕ for the hole array of d = 1.2, a = 2.0, and t = 0.5 mm, and found $\phi = -0.98\pi$ at the peak frequency. The approximate $-\pi$ phase change reveals the oscillations of the acoustic field on the front and rear surfaces of the plate are out-of-phase, which is distinct from the corresponding characteristic in the EM case. For EM wave transmitted through a hole array, the hole acts as barrier due to the transmission frequency much lower than the cutoff frequency of the hole, and the wave has to tunnel through the hole in a form of evanescent field. So the phase change of the EM wave across the holey film/plate assumes nearly zero [37]. This difference in transmission phase bares the distinct behaviors of a hole to acoustic and EM waves, again.

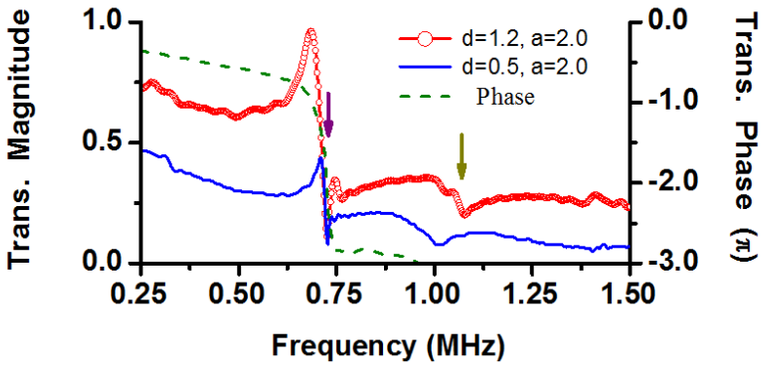

Figure 2. Acoustic transmissions at normal incidence through the hole arrays with the same lattice constant, 2.0 mm, and the same thickness, 0.5 mm, but different diameters as denoted. The measured transmission phase curve is for the hole array: d = 1.2, a = 2.0, and t = 0.5 mm. The arrows indicate the Wood's anomalies, $\lambda = a$ and $\lambda = a/\sqrt{2}$. Reprinted with permission from J. Appl. Phys. 104, 014909 (2008). Copyright 2008 American Institute of Physics.

Figure 3 shows the transmission spectra at oblique incidence measured with the incident angle θ varying from 0° to 25° for the hole array of d = 1.2, a = 2.0, and t = 0.5 mm. The transmission map is plotted as a function of both the frequency and the incidence angle. The predicted variation of Wood's anomalies versus angle is plotted as solid lines and is superposed on the map. Derived from the conservation of momentum, the variation relation reads:

$$af^{(l,m)}/c = \left(l\sin\theta + \sqrt{l^2 + m^2\cos^2\theta}\right)/\cos^2\theta \tag{2}$$

for the Wood's anomaly frequency $f^{(l,m)}$ of order (l, m). It is seen from the map that the measured shifting of Wood's anomalies with the incidence angle agrees well with the solid

lines. On the other hand, the peaks exhibit a strong angle-dependent behavior in the same way as Wood's anomalies.

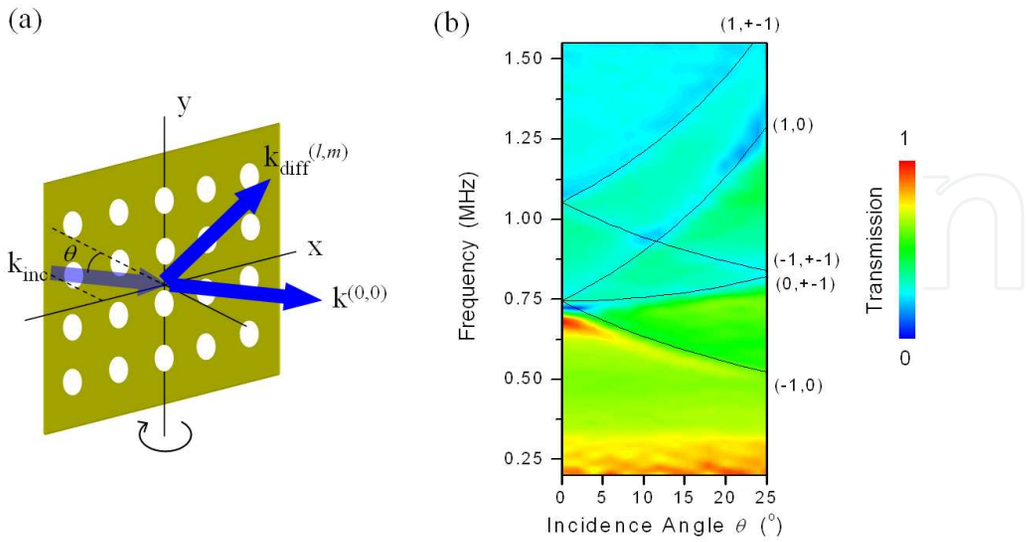

Figure 3. (a) The schematic picture of oblique incidence of acoustic waves. The wave vector $\mathbf{k}_{inc}$ represents the incident wave illuminating the hole array at the incidence angle θ. The obliquity occurs along the [1,0] direction of the array. The wave vector $\mathbf{k}^{(0,0)}$ represents the (0,0)-order transmitted wave. The wave vector $\mathbf{k}_{diff}^{(l,m)}$ represents the (l,m)-order diffraction wave. (b) Acoustic transmission magnitude plotted as a function of the wave frequency and the incidence angle for the hole array, d = 1.2, a = 2.0, and t = 0.5 mm. The solid lines superposed are the variation curves of Wood's anomalies with the incidence angle. Reprinted with permission from J. Appl. Phys. 104, 014909 (2008). Copyright 2008 American Institute of Physics.

In recent investigations, it is demonstrated that the SF resonance can be responsible for enhanced transmissions of EM waves through subwavelength hole arrays [26,27]. We have considered that the acoustic surface wave at the brass-water interface might play no role in the present transmission phenomenon, and shown that the SF resonance holds for acoustic waves by generalizing the proof of EM waves [38,39]. The SF resonance has some spectral features: the resonant wavelength is determined essentially by the lattice constant and is very sensitive to the incidence angle with accompanied by Wood's anomalies. Here, the experimental results for the enhanced acoustic transmission through the hole array in the 0.5 mm thick plate manifests the features of SF resonance.

When the plate thickness becomes larger, the situations begin to divide for two types of waves. For EM wave, the transmission peak will diminish after the metallic film/plate becomes thick enough, because the holes have the cutoff. In sharp contrast, there is no cutoff for acoustic waves to propagate through the holes. When the thickness is large enough, for instance t = 2.3 mm, there can be multiple transmission peaks well below the Wood's anomaly, as shown in Figures 4(a) and 4(b). The measured spectra show the typical characteristics of FP resonance in terms of the phase values at the transmission maxima and minima. From Figure 4(c), the peaks are not sensitive to the incidence angle. In fact, these transmission peaks are caused by standing-wave-formed resonances of the acoustic wave

establishing inside the hole channel. However, these resonances undergo a tuning, to some degree, by diffraction evanescent waves parasitical to a grating, and consequently deviate from the ordinary FP conditions while the plate thickness becomes comparable to the lattice constant, which will be further discussed later.

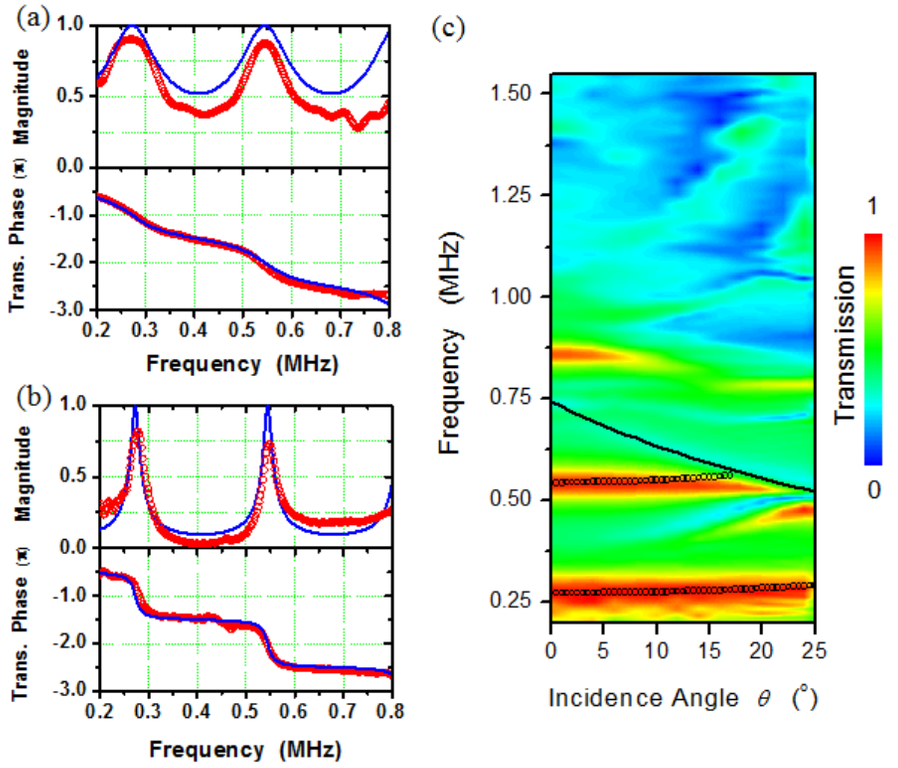

Figure 4. (a) Normal transmission of acoustic waves through the hole array (open circles), d = 1.2, a = 2.0, and t = 2.3 mm, immersed in water and through the effective fluid layer (solid line) immersed in water alike. Open circles are the measurement data, and the solid lines are the calculation based on the effective fluid model with $\overline{n} = 1.19$ and $\overline{\eta} = 0.28\eta_{water}$. (b) Normal transmission for the hole array, d = 0.5, a = 2.0, and t = 2.3 mm. Open circles are the measurement data, and the solid lines are the calculation based on the effective fluid model with $\overline{n} = 1.19$ and $\overline{\eta} = 0.05\eta_{water}$. (c) Acoustic transmission magnitude plotted as a function of the wave frequency and the incidence angle for the hole array d = 1.2, a = 2.0, and t = 2.3 mm. The obliquity occurs along the [1,0] direction of the array. The solid line superposed are the variation curve of Wood's anomaly (-1,0) with the incidence angle. The open circles superposed denote the variation of the transmission peaks, calculated from the FP resonance condition of the effective fluid model at oblique incidence. Reprinted with permission from J. Appl. Phys. 104, 014909 (2008). Copyright 2008 American Institute of Physics.

3.2. Enhanced transmission of acoustic waves through bull's eye structure

Soon after the discovery of extraordinary optical transmission through a metallic film with two-dimensional array of sub-wavelength holes, it was found that there can be enhanced and collimated transmission through a single sub-micron hole surrounded by finite periodic rings of indentations (denoted as bull's eye) [4]. We also examined the transmission of a bull's eye structure for acoustic waves. The bull's eye structure, shown in the inset of Figure

5, was fabricated by patterning both sides of a thin brass plate with concentric periodic grooves around a single cylindrical hole. The thickness of the brass plate is 1.6 mm, and the diameter of the central hole is 0.5 mm. The groove period is 2.0 mm, and there are a total of 15 grooves. The width and depth of each groove are 0.5 mm and 0.3 mm, respectively.

In Figure 5, we showed the measured transmittances as a function of frequency for both bull's eye structure and the reference sample (a smooth brass plate of the same thickness). It can be seen that there is a transmission peak at 0.71 MHz for bull's eye structure, while such peak is missing for the reference sample. In Figure 5, we also plotted the power transmittance calculated by using COMSOL MULTIPHYSICS, a commercial finite-element solver. It can be seen that the predicted peak position agrees well with the experimental data. However, the measured transmittance is much lower than that predicted and the precise reason for this disagreement is yet to be uncovered.

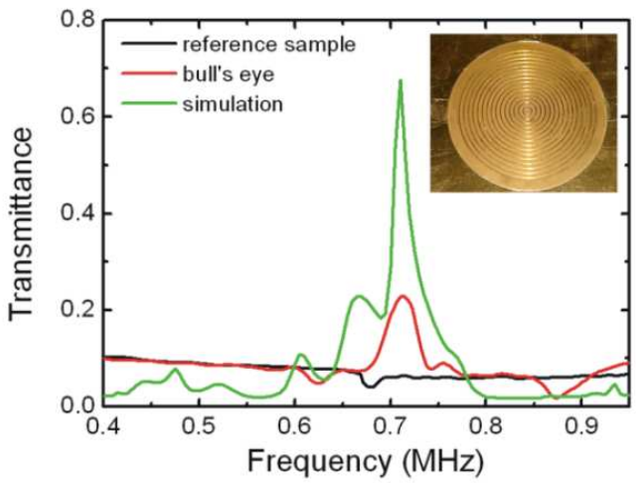

Figure 5. Measured transmittances for both the bull's eye structure and the reference sample, together with calculated power transmittance for bull's eye. Inset shows an image of the sample, fabricated by patterning both sides of a thin brass plate with concentric periodic grooves around a single cylindrical hole. The thickness of the brass plate is 1.6 mm, and the diameter of the central hole is 0.5 mm. The groove period is 2.0 mm, and the groove width and depth are 0.5 mm and 0.3 mm, respectively. Reprinted with permission from Appl. Phys. Lett. 92, 124106 (2008). Copyright 2008 American Institute of Physics.

For ultrasonic waves in water, wavelength corresponding to 0.71 MHz is 2.1 mm, which is slightly larger than the groove period of bull's eye, 2.0 mm. This close correspondence is a strong clue indicating that the enhanced transmittance is due to the diffraction effect. It has been shown that enhanced acoustic wave transmission through hole arrays in perfectly rigid thin plate, where there can be no surface wave, may be related (and understood via Babinet's principle) to "resonant" reflection by its complementary structure, i.e., planar arrays of perfectly rigid disks [26, 39]. In fact, both were found to be associated with the *divergence* in the scattering structure factor, owing to the coherent addition of the Bragg scattering amplitudes from the periodic array of holes or disks. As a result, a quasi surface mode with frequency close to the onset of the first diffraction order (wavelength λ slightly larger than the lattice constant a) always exists. Such modes are denoted "structure-factor-

induced surface modes," or SF resonances. Since diffraction is the ultimate mechanism for the SF resonances, we expect the same to also apply to bull's eye structure, which can be viewed as having 1D periodicity along the radial direction.

Besides the transmission enhancement, the collimation effect of the bull's eye structure is very striking [4,40]. As shown in Figure 6(a), the far-field acoustic wave on the transmission side is also in the form of a tight beam with a lateral dimension not exceeding the groove periodicity. The full width at half maximum (FWHM) divergence is $\pm 2^{o}$. As analyzed above, it is the coherent scattering which leads to the emergence of a strongly collimated beam in the far-field region. In Figures 6(b) and 6(c) we also plotted the scanned results at a distance of about 15 wavelengths from the transmission side of the surface, for both the bull's eye structure and the reference sample. Compared with the reference sample, the collimation effect for bull's eye structure is very evident. In addition, it is found by simulation that both the intensity of the acoustic wave field around the central hole region, as well as the collimation effect, would increase with the number of concentric grooves. This is reasonable, since the coherent scattering effect becomes stronger if more concentric grooves are involved.

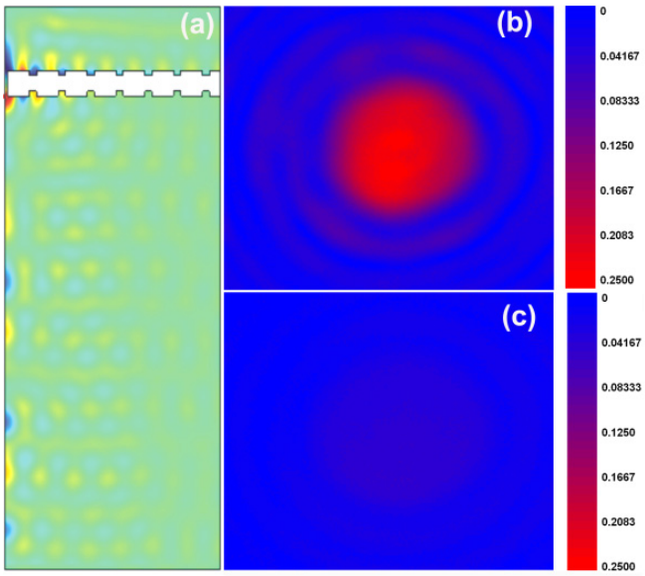

Figure 6. (a) Calculated far-field pressure amplitude distribution at 0.71 MHz in the axial symmetry coordinates. (b) Experimentally scanned far-field (~15 wavelengths from the transmission side of the plate surface) pressure magnitude distributions in an area of 40×40 mm^2, for the bull's eye structure at 0.71 MHz. (c) Same as (b), for the reference sample. Reprinted with permission from Appl. Phys. Lett. 92, 124106 (2008). Copyright 2008 American Institute of Physics.

4. Discussions

4.1. Fabry-Perot resonances tuned via diffraction evanescent waves

For the hole arrays, we measured the acoustic samples with various plate thicknesses ranging from 0.5 mm to 3.1 mm, as plotted in the inset of Figure 7. In theory, we employed the mode expansion method to calculate analytically the transmission [39]. We found that the observed transmission peaks are the manifestation of a type of resonance mode that has

FP and SF resonances as the two limits. The diffraction evanescent modes play an important role in interpolating between the two limits. To make explicit the role of diffraction evanescent waves, we retained the lowest cylindrical mode inside the holes and 5 lowest plane wave modes outside the holes, and obtained the resonant mode equation as

$$\tan(2t\omega/c) = \frac{-a^3 k_0 k_1^2}{\frac{\pi(1-\xi^2)}{16J_1^2(2\pi r/a)} a^3 k_1^3 + \pi^2 \frac{2a}{t}}, \tag{3}$$

in which $k_0 = \omega/c = 2\pi f/c$, $k_1 = \sqrt{(2\pi/a)^2 - (\omega/c)^2}$ is the diffraction evanescent wavevector, and J_1 is the first order Bessel function. Equation (3) is instructive, since a vanishing right-hand side would directly yield the FP resonance condition $t = n\lambda/2$, λ being the wavelength. A combination of hole and periodic diffraction evanescent wave effects constitute the correction to the usual FP condition in the form of a non-zero right hand side, implying that the FP resonance can be tuned by varying the periodicity and area fraction of holes. We denote such resonances the FPEV resonances.

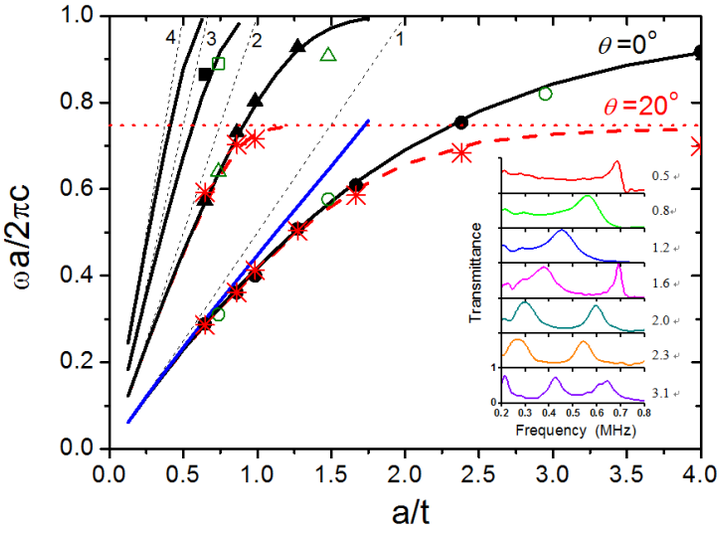

Figure 7. Solid symbols (measurement) and black solid lines (calculation) are the resonant transmission frequencies of normally incident acoustic wave through a square lattice of holes with $r = 0.3a$. Star symbols (measurement) and red dashed lines (calculation) denote the case of acoustic wave at 20° incidence angle along [0,1] direction, for which the Wood's anomaly frequency is the horizontal dot line. Black dashed lines delineate the FP condition with the order n denoted. Blue line is determined by Equation (3), with a slope of ~0.42 (i.e. $t \approx 0.42\lambda$). Open symbols represent the measured transmission peaks of normally incident microwave on a metallic grating, 1D periodic slits, with area fraction 0.32. The inset shows the measured acoustic transmittances at normal incidence for various plate thicknesses, with a = 2.0 mm and r = 0.6 mm. The thickness (in mm) of each plate is given to the right of the spectrum. Reprinted with permission from Phys. Rev. B 76, 054303 (2007). Copyright 2007 by The American Physical Society.

In Figure 7 we show the measured and calculated FPEV resonance frequencies plotted as a function of inverse plate thickness. The FP condition is indicated by the black dashed

straight lines, for n=1, 2, 3, 4, with slopes of 0.5, 1, 1.5 and 2, respectively. The FPEV frequencies are shown as solid black (normal incidence), and red dashed (20^o oblique incidence) lines. Compared with the FP resonances, it is seen that the FPEV resonances always occur at lower frequencies, as though the effective plate thickness is greater than t. The prediction of Equation (3), for the n=1 FPEV resonance, is shown as the blue line. Except in the region of very small a/t values, the blue line has a slope of 0.42. Thus the effect of the diffraction evanescent waves is to shift the resonance condition by ~16%, in the direction of smaller channel length. The difference between the prediction of Equation (3) and the black lines appears at the small t limit, where the transmission peak frequency shows a clear dependence on the incidence angle. This is characteristic of the surface-wave-like mode induced by the SF resonance. In fact, these transmission peak frequencies all occur at close to the Wood's anomaly, as required by the SF resonance condition. Thus the lowest frequency FPEV resonance, which shows little or no dependence on the incidence angle, is smoothly converted to the structure-factor-induced surface mode in the thin-plate limit. The diffraction evanescent wave contributions are dominant at the intermediate values of a/t. To a lesser degree, similar behavior can be observed for the higher order FPEV's.

It is seen that as the ratio a/t increases, the lowest order evanescent waves (Equation (3)) can no longer account for the resonant frequency trajectory. Also, in the large a/t limit the curves also display pronounced incident angle dependence, in contrast to FP resonances which are nearly independent of the incidence angle. These are the signals for (1) the lateral scattering interaction is contributing much more to the resonant modes, hence the lowest order evanescent modes are no longer sufficient to account for such strong lateral interactions, and (2) with the increased lateral interaction, SF effect becomes more pronounced, implying incidence angle dependence. These spectral features also correspond to the different field distributions, as shown in Figure 8, where the surface field is localized on the holes for FP-like resonances and the interference pattern is seen in the region between the holes for SF resonances.

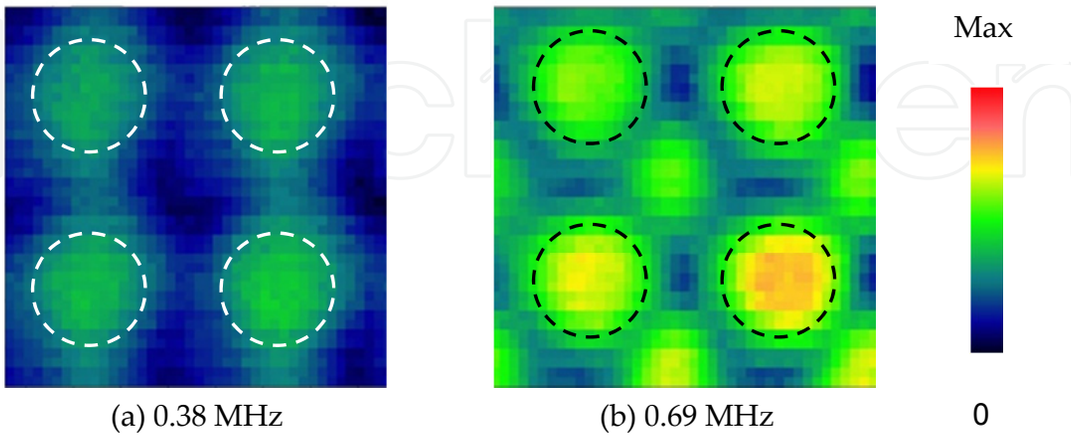

Figure 8. The measured distribution of pressure field at the rear surface of the hole array a =2.0, r =0.6, and t =1.6 mm for two resonance frequencies 0.38MHz (a/λ=0.51) and 0.69MHz (a/λ=0.93). The holes are delineated by dashed lines.

It is interesting to note that the transmission of microwave through a metallic grating of 1D slits has the similar FPEV resonances for the incident polarization with E-field perpendicular to the silts, see open symbols in Figure 7 [37]. This is because the slits have no cutoff to the perpendicular polarization of EM waves, in the same physics as the holes to acoustic waves.

4.2. The effective fluid model for thick plates

For a very small *a*/*t* ratio, these resonance wavelengths are much larger than the lattice constant, allowing us to take a view of effective media. Here we employ a simple argument in the same fashion as the EM case [41] with the assumption of brass plate being rigid, and find that the hole array structure fabricated in a rigid plate and filled with a fluid (mass density ρ_0 and bulk modulus κ) may be viewed as an effective fluid with the same thickness, effective mass density $\overline{\rho}_0$ and bulk modulus $\overline{\kappa}$. It is known that the acoustic wave is characterized by the pressure field, p, and velocity field, $\boldsymbol{u}$. Averaging the pressure field in the holes, we get the effective pressure field in the effective fluid $\overline{p} = \xi p$. Requiring the acoustic energy flow across the surface to be the same for the hole array and the effective fluid, i.e. $p\boldsymbol{u} \cdot \pi d^2 / 4 = \overline{p}\,\overline{\boldsymbol{u}} \cdot a^2$, we obtain the effective velocity $\overline{\boldsymbol{u}} = \boldsymbol{u}$. Also the total acoustic energy for both systems are required to be the same, $\left(\frac{1}{2}\rho_0 \boldsymbol{u}^2 + \frac{1}{2}p^2 / \kappa\right) \cdot \pi d^2 / 4 \cdot t = \left(\frac{1}{2}\overline{\rho}_0 \overline{\boldsymbol{u}}^2 + \frac{1}{2}\overline{p}^2 / \overline{\kappa}\right) \cdot a^2 \cdot t$, which gives us the effective parameters $\overline{\rho}_0 = \xi \rho_0$ and $\overline{\kappa} = \xi \kappa$. Thereafter, the acoustic speed and impedance of the effective fluid are $\overline{v} = v = \sqrt{\kappa / \rho_0}$ and $\overline{\eta} = \xi\eta = \xi\sqrt{\rho_0 \kappa}$, where v and η are the acoustic speed and impedance of the filling fluid, respectively. The relations indicate the acoustic speed remains unchanged and the impedance is scaled by a factor of the area fraction of holes for the effective fluid.

The above argument is applicable under long wavelength limit ($a/\lambda \to 0$) where diffraction evanescent waves are negligible. For the sample with thickness comparable to lattice constant, the diffraction evanescent waves tune the FP resonances and the resultant transmission resonances can occur for channel length ~16% thinner than required by the FP resonances. Superficially, this diffractive effect is substitutable by a slowing of acoustic wave propagation inside the holes, i.e. $v = 0.84c$. Based on the above argument, the effective fluid equivalent to a 2.3 mm thick sample has the acoustic speed $\overline{v} = v = 0.84c$, or the acoustic refractive index $\overline{n} = c / \overline{v} = 1.19$, and the effective impedance $\overline{\eta} = \xi\eta = \xi\eta_{water}$. With these two effective parameters at hand, we calculated the transmission spectra, both magnitude and phase, of the effective fluid layer at normal incidence according to the formula:

$$T\exp(j\phi) = \frac{1}{\cos(k_0 \overline{n} t) + \frac{j}{2}\left(\frac{\overline{\eta}}{\eta_{water}} + \frac{\eta_{water}}{\overline{\eta}}\right)\sin(k_0 \overline{n} t)} \tag{4}$$

where $k_0 = 2\pi f / c$ is the wavenumber of the incidence wave. The calculated results (solid lines) are shown in Figures 4(a) and 4(b) to compare with the experimental data (open circles) for two samples with identical thickness 2.3 mm, and identical lattice constant 2.0 mm, but different hole diameters 1.2 and 0.5 mm. Good agreement between the calculations and the experiments is seen at the frequencies below the Wood's anomaly (0.75 MHz), which verifies the applicability of the effective fluid model at normal incidence.

In Figure 4(c), we see two flat bands appear below 0.75 MHz, and they are the first and second FP resonances, see Figure 4(a) where the phase values indicate the order of FP resonances. The open circles superimposed are the variations of the transmission peaks of the effective fluid layer which are obtained from the FP resonance condition at oblique incidence, $\sin\left[k_o \overline{n} t\sqrt{1-\left(\sin\theta / \overline{n}\right)^2}\right] = 0$. The agreement between the calculated variations of the transmission peaks and the measured results indicates the applicability of the effective fluid model persists to a range of incidence angle. The discrepancy at θ >15° for the second FP transmission peak is due to the emerging of the (-1,0) diffraction order nearby, and the red flat band is seen to terminate upon crossing with Wood's anomaly (-1,0). Where the cross happens, there will be the strong coupling interaction between SF resonance of the array and FP-like resonance localized at each hole, which possibly gives rise to the 0.48 MHz band at θ =25°.

The effective fluid model allows us to use the holey or slotted hard plate to realize an acoustic medium, and provides some freedom to design acoustic materials, because some material parameters, difficult to be tuned, are related simply to the structural factors of the hole array or the slits. In Figure 9, we illustrated conceptually an acoustic prism made of such slotted hard plate. A detailed discussion is seen in reference [42].

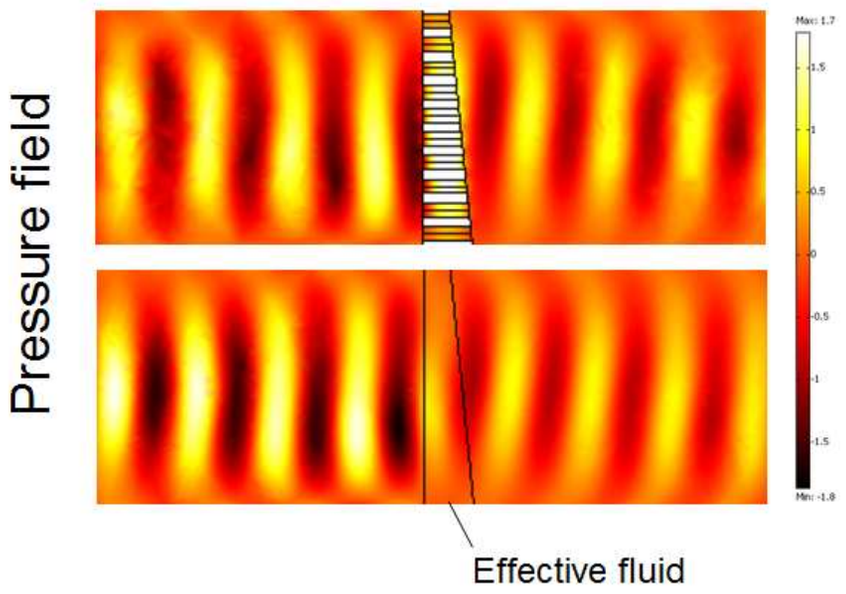

Figure 9. Simulation results for a structured hard plate (upper) with tapered thickness to function as the acoustic prism. The pressure field is compared with a fluid with the effective parameters (lower).

5. Conclusion

We investigated experimentally the acoustic transmission through subwavelength holes fabricated on brass plates at normal and oblique incidence within ultrasonic frequencies regime. The transmission phenomena for both hole array and bull's eye structure in thin brass plates, analogous to the observed enhanced transmission of EM waves through subwavelength hole arrays in a metallic film, exhibit the transmission enhancement because of the SF resonance. At the peak frequency, the transmission phase is nearly $-\pi$, indicating the out-of-phase oscillations of the acoustic field at two surfaces of the plate. For the hole array in thick brass plates, the transmission peaks of acoustic waves are related to the FP-like resonances inside the holes and therefore occur well below Wood's anomaly, since a hole has no cutoff frequency for acoustic propagation. By varying the plate thickness or channel length, one makes the transition from the FP resonance (thick plate limit) to the SF resonance (thin plate limit). Between the two limits there can be interesting deviation from FP resonance conditions, owing to the interaction of the diffraction evanescent waves. In the case of thick plates, the structure can be viewed as a new fluid with effective mass density and bulk modulus scaled, under long wavelength limit, by a factor of area fraction of the holes. The effective medium model describes well the transmission properties of the hole array within a range of incidence angle.

Our discussion assumed the approximation of hard plates and did not take acoustic surface waves into account. With acoustic surface waves being involved, transmissions of acoustic waves through structured plates have found far richer and more complicated physical phenomena in the past few years and will attract more attentions in the future [43-45]. Although this subject is an old problem, its new phenomena may appear from time to time and the underlying mechanism waits to be unlocked.

Author details

Bo Hou
School of Physical Science and Technology, Soochow University, Suzhou, Jiangsu, China

Weijia Wen
Department of Physics, Hong Kong University of Science and Technology, Clear Water Bay, Kowloon, Hong Kong, China

Acknowledgement

We would like to thank our collaborators in this project. B. Hou is supported by the National Natural Science Foundation of China (Grant No. 11104198) and a Project Funded by the Priority Academic Program Development of Jiangsu Higher Education Institutions (PAPD). W. Wen is supported by RGC Grant HKUST2/CRF/11G.

6. References

[1] Bethe H. A. (1944) Theory of diffraction by small holes, Phys. Rev. 66: 163.
[2] Roberts A. (1987) Electromagnetic theory of diffraction by a circular aperture in a thick, perfectly conducting screen, J. Opt. Soc. Am. A 4: 1970.
[3] Ebbesen T. W., Lezec H. J., Ghaemi H. F., Thio T., and Wolff P. A. (1998) Extraordinary optical transmission through subwavelength hole arrays, Nature 391: 667.
[4] Lezec H. J., Degiron A., Devaux E., Linke R. A., Martin-Moreno L., Garcia-Vindal F. J., and Ebbesen T. W. (2002) Beaming light from a subwavelength aperture, Science 297: 820.
[5] Ghaemi H. F., Thio T., Grupp D. E., Ebbesen T. W., and Lezec H. J. (1998) Surface plasmons enhance optical transmission through subwavelength holes, Phys. Rev. B 58: 6779.
[6] Grupp D. E., Lezec H. J., Ebbesen T. W., Pellerin K. M., and Thio T. (2000) Crucial role of metal surface in enhanced transmission through subwavelength apertures, Appl. Phys. Lett. 77: 1569.
[7] Krishnan A., Thio T., Kim T. J., Lezec H. J., Ebbesen T. W., Wolff P. A., Pendry J., Martin-Moreno L., and Garcia-Vidal F. J. (2001) Evanescently coupled resonance in surface plasmon enhanced transmission, Opt. Commun. 200: 1.
[8] Martín-Moreno L., García-Vidal F. J., Lezec H. J., Pellerin K. M., Thio T., Pendry J. B., and Ebbesen T. W. (2001) Theory of extraordinary optical transmission through subwavelength hole arrays, Phys. Rev. Lett. 86: 1114.
[9] Martín-Moreno L. and García-Vidal F. J. (2004) Optical transmission through circular hole arrays in optically thick metal films, Opt. Express 12: 3619.
[10] Barnes W. L., Murray W. A., Dintinger J., Devaux E., and Ebbesen T. W. (2004) Surface plasmon polaritons and their role in the enhanced transmissions of light through periodic arrays of subwavelength holes in a metal film, Phys. Rev. Lett. 92: 107401.
[11] Barnes W. L., Dereux A., and Ebbesen T. W. (2003) Surface plasmon subwavelength optics, Nature 424: 824.
[12] Genet C. and Ebbesen T. W. (2007) Light in tiny holes, Nature 445: 39.
[13] Garcia-Vidal F. J., Martin-Moreno L., Ebbesen T. W., and Kuipers L. (2010) Light passing through subwavelength apertures, Rev. Mod. Phys. 82: 729.
[14] Porto J. A., Garcia-Vidal F. J., and Pendry J. B. (1999) Transmission resonances on metallic gratings with very narrow slits, Phys. Rev. Lett. 83: 2845.
[15] Rosenberg A. and Bolden E. A. (2000) Optical filters consisting of metallic waveguide arrays, J. Opt. Soc. Am. A 17: 1461.
[16] Fan W., Zhang S., Minhas B., Malloy K. J., and Brueck S. R. (2005) Enhanced infrared transmission through subwavelength coaxial metallic arrays, Phys. Rev. Lett. 94: 033902.
[17] Bonod N., Enoch S., Li L., Popov E., and Neviere M. (2003) Resonant optical transmission through thin metallic films with and without holes, Opt. Express 11: 482.
[18] Baida F. I. and Van Labeke D. (2002) Light transmission by subwavelength annular aperture arrays in metallic films, Opt. Commun. 209: 17.

[19] Quemerais P., Barbara A., Le Perchec J., and Lopez-Rios T. (2005) Efficient excitation of cavity resonances of subwavelength metallic gratings, J. Appl. Phys. 97: 053507.
[20] Suckling J. R. and Sambles J. R. (2005) Remarkable zeroth-order resonant transmission of microwaves through a single subwavelength metal slit, Phys. Rev. Lett. 95: 187407.
[21] Matsui T., Agrawal A., Nahata A., and Vardeny Z. V. (2007) Transmission resonances through aperiodic arrays of subwavelength apertures, Nature 446: 517.
[22] Rivas J. G., Janke C., Bolivar P. H., and Kurz H. (2005) Transmission of THz radiation through InSb gratings of subwavelength apertures, Opt. Express 13: 847.
[23] Azad A. K., Zhao Y., and Zhang W., (2005) Transmission properties of terahertz pulses through an ultrathin subwavelength silicon hole array, Appl. Phys. Lett. 86: 141102.
[24] Wen W., Zhou L., Hou B., Chan C. T., and Sheng P. (2005) Resonant transmission of microwave through subwavelength fractal slits in a metallic plate, Phys. Rev. B 72: 153406.
[25] Ruan Z. and Qiu M. (2006) Enhanced transmission through periodic arrays of subwavelength holes: The role of localized waveguide resonances, Phys. Rev. Lett. 96: 233901.
[26] García de Abajo F. J., Gómez-Medina R., and Sáenz J. J. (2005) Full transmission through perfect-conductor subwavelength hole arrays, Phys. Rev. E 72: 016608.
[27] García de Abajo F. J. (2007) Light scattering by particle and hole arrays, Rev. Mod. Phys. 79: 1267.
[28] van der Molen K. L., Klein Koerkamp K. J., Enoch S., Segerink F. B., van Hulst N. F., and Kuiperts L. (2005) Role of shape and localized resonances in extraordinary transmission through periodic arrays subwavelength holes : experiment and theory, Phys. Rev. B 72: 045421.
[29] Cao H. and Nahata A. (2004) Influence of aperture shape on the transmission properties of a periodic array of subwavelength apertures, Opt. Express 12: 3664.
[30] Spence R. D. (1948) The diffraction of sound by circular disks and apertures, J. Acoust. Soc. Am. 20: 380.
[31] Lamb H., *Hydrodynamics*, 6th ed. (Dover, New York, 1991)
[32] Miles J. (2002) On resonant reflection by a plane grating, Wave Motion 35: 311.
[33] Wilson G. P. and Soroka W. W. (1965) Approximation to the diffraction of sound by a circular aperture in a rigid wall of finite thickness, J. Acoust. Soc. Am. 37: 286.
[34] Seo J. S., Eom H. J., and Lee H. S. (2000) Acoustic scattering from two circular apertures in a thick hard plane, J. Acoust. Soc. Am. 107: 2338.
[35] Zhang X. (2005) Acoustic resonant transmission through acoustic gratings with very narrow slits: Multiple-scattering numerical simulations, Phys. Rev. B 71: 241102(R).
[36] Lu M. H., *et al*. (2007) Extraordinary acoustic transmission through a 1D grating with very narrow apertures, Phys. Rev. Lett. 99: 174301.
[37] Hou B. and Wen W. (2008) Transmission resonances of electromagnetic wave through metallic gratings: phase and field characterizations, Opt. Express 16: 17098.
[38] Here, acoustic surface wave refers to a type of elastic interface wave, Stoneley wave, which can be excited at the interface between a solid material and a fluid, though the

surface-wave-like mode induced by the structure factor may be defined on structured surfaces made of ideally conducting/rigid material.

[39] Hou B., Mei J., Ke M., Wen W., Liu Z., Shi J., and Sheng P. (2007) Tuning Fabry-Perot resonances via diffraction evanescent waves, Phys. Rev. B 76: 054303.

[40] Christensen J., Fernandez-Dominguez A. I., de Leon-Perez F., Martin-Moreno L., and Garcia-Vidal F. J. (2007) Collimation of sound assisted by acoustic surface waves, Nature Physics 3: 851.

[41] Shen J. T., Catrysse P. B., and Fan S. (2005) Mechanism for designing metallic metamaterials with a high index of refraction, Phys. Rev. Lett. 94: 197401.

[42] Cai F., Liu F., He Z., and Liu Z. (2007) High refractive-index sonic material based on periodic subwavelength structure, Appl. Phys. Lett. 91: 203515.

[43] Estrada H., García de Abajo F. J., Candelas P., Uris A., Belmar F., and Meseguer F. (2009) Angle-dependent ultrasonic transmission through plates with subwavelength hole arrays, Phys. Rev. Lett. 102: 144301.

[44] Zhou Y., *et al*. (2010) Acoustic surface evanescent wave and its dominant contribution to extraordinary acoustic transmission and collimation of sound, Phys. Rev. Lett. 104: 164301.

[45] He Z., *et al*. (2010) Acoustic transmission enhancement through a periodically structured stiff plate without any opening, Phys. Rev. Lett. 105: 074301.